Astron. Astrophys. 211, 463–475 (1989)

ASTRONOMY AND ASTROPHYSICS

# The internal magnetic field distribution and the diameters of solar magnetic elements

**I. Zayer[1], S.K. Solanki[2,★], and J.O. Stenflo[3,★★]**

[1] Institute of Astronomy, ETH-Zentrum, CH-8092 Zürich, Switzerland
[2] Department of Applied Mathematics, University of St. Andrews, St. Andrews KY16 9SS, Scotland
[3] High Altitude Observatory, P.O.Box 3000, Boulder, CO 80307, USA

Received June 27, accepted September 16, 1988

**Summary.** A new diagnostic for the horizontal distribution and vertical gradient of the magnetic field within spatially unresolved solar magnetic elements is presented. It is based on the width of the individual Stokes $V$ $\sigma$-components of a completely Zeeman split line in the infrared (Fe I $\lambda$ 15648.54 Å), and on a comparison with the Stokes $V$ profiles of 3 other lines including the traditional line ratio technique pair in the visible (Fe I $\lambda$ 5247.1 Å and $\lambda$ 5250.2 Å). Extensive radiative transfer calculations are carried out to model the magnetic field structure, which is fitted to observational data acquired with a Fourier transform spectrometer.

The data can only be explained by a variation in magnetic field strength. A purely horizontal variation of the magnetic field cannot reproduce all the data simultaneously, so that a magnetic field whose strength decreases with height is required. An appropriate vertical gradient of the magnetic field alone is, on the other hand, sufficient, suggesting that in the lower photosphere the field strength inside fluxtubes is horizontally almost constant and that most fluxtubes in the resolution element have very similar field strengths. The thin tube approximation is found to be a reasonable representation of the vertical variation of the field strength, with the field strength at continuum optical depth unity inside magnetic elements being approximately 2000 G.

The shape of the $\sigma$-components of the fully split $\lambda$ 15648.54 Å line suggests the presence of a small amount of flux in either weak-field form (400 G) with the same polarity as the stronger fluxtube fields, or of medium strength (800 G) bearing opposite polarity. The presented calculations favour the opposite polarity field. A possible scenario which may explain the observations consists of a fluxtube model with a small return flux, in which about 3–7% of the flux is directed back to the surrounding regions.

The magnetic field structure derived from the simultaneous analysis of infrared and visual data at disk centre also reproduces data near $\mu = 0.6$. The comparison of the results at the two disk positions allows, for the first time, some preliminary constraints to be set on fluxtube diameters independently of the spatial resolution of the observations. If a slab geometry is assumed for the fluxtubes, then an average fluxtube full width of 60–100 km at the $\tau = 1$ level is found in an active region plage, while for a cylindrical fluxtube the diameter is found to be approximately 300 km. It is shown that for a given geometry the fluxtubes in the resolution element must have similar widths.

A sizeable turbulence velocity (combination of micro- and macroturbulence) of 3–3.4 km s$^{-1}$ inside the magnetic elements is derived from the infrared lines.

**Key words:** solar magnetic fields – fluxtubes – Stokes parameters – line profiles – infrared spectra

## 1. Introduction

Theoretical models of small (i.e. with diameters less than 1 arc sec) solar magnetic fluxtubes have magnetic fields with strengths of 1–2 kG in the lower photosphere (e.g. Spruit, 1979; Deinzer et al., 1984a,b; Hasan, 1985; Steiner et al., 1986). Below the chromosphere the main confining agent of the field is the gas pressure. Accordingly, the field strength in these models decreases with height not too differently from the thin tube approximation, i.e. the field strength follows approximately from the pressure difference between the inside of the fluxtube and its non-magnetic surroundings (Pneuman et al., 1986; Knölker et al., 1988). As far as the horizontal variation of the field is concerned, theoretical models tend to be much more varied, with a radially uniform field strength within the fluxtube (e.g. Defouw, 1976; Roberts and Webb, 1979; Hasan, 1985), a potential field distribution (e.g. Spruit, 1976), a Gaussian distribution (e.g. Osherovich et al., 1983), a quadratic distribution (Pneuman et al., 1986), or the distribution resulting from a fully self-consistent solution of the MHD equations starting from various profiles at the lower boundary (Deinzer et al., 1984a,b; Steiner et al., 1986), all being present in the literature.

Although the field strength at a given level in the fluxtubes is well determined by observations, so far they have been able to constrain the horizontal and vertical variation of the field only either indirectly or qualitatively. The main aim of the present paper is to set more quantitative constraints on these parameters. In addition we set some preliminary constraints on the diameters

*Send offprint requests to:* I. Zayer
★ Permanent address: Institute of Astronomy, ETH-Zentrum, CH-8092 Zürich, Switzerland
★★ Visiting astronomer, National Solar Observatory. Operated by the Association of Universities for Research in Astronomy, Inc., under contract with the National Science Foundation

of small fluxtubes and on the non-stationary velocity amplitudes in their deeper photospheric layers.

The most widely used diagnostic of the magnetic field strength in solar magnetic fluxtubes has been the line ratio technique, which compares simultaneously recorded Stokes $V$ profiles (i.e circular polarisation spectra) of two lines in the visible with different Zeeman splitting, but otherwise very similar properties (Stenflo, 1973; Wiehr, 1978; Frazier and Stenflo, 1978; Stenflo and Harvey, 1985; Solanki et al., 1987). Other magnetic field strength diagnostics include the Fourier transform of the Stokes $V$ profile (e.g. Tarbell and Title, 1976, 1977), the Fourier transform of the Stokes $I$ profiles of two selected lines (Robinson et al., 1980) and the statistical analysis of a large number of Stokes $V$ profiles (Solanki and Stenflo, 1984). Yet another approach consists of directly examining the Zeeman splitting of an infrared line, e.g. around 1.5 $\mu$m, where, in contrast to the visible, the splitting of a solar $g = 3$ line is complete in a kG magnetic field due to the increase of the Zeeman splitting with the square of the wavelength. Observations by Harvey and Hall (1975) [see also Harvey, 1977] revealed the powerful potential of this method, although inadequate spectrometers and infrared detectors prevented its use to a fuller extent until recently.

Although these methods have provided values of the inherent field strength at some height in the fluxtubes they cannot, in the forms used so far, constrain the lateral and vertical distribution of the magnetic field. Thus it was shown by Stenflo (1973) and Frazier and Stenflo (1978) that the line ratio technique cannot distinguish between various horizontal distributions of the magnetic field strength. A horizontal distribution of the field has only been measured in sunspots and pores (e.g. Beckers and Schröter, 1969; Abdussamatov, 1971; Lites et al., 1988; Deming et al., 1988), although Knölker et al. (1988) do provide some indirect evidence, based on continuum contrasts, for a horizontally constant field and a relatively narrow boundary layer at the $\tau = 1$ level in magnetic elements. Measurements of the vertical value of the magnetic field have generally only given some gradient averaged over a considerable height range, often derived by comparing lines formed at different heights (e.g. Henze et al., 1982; Hagyard et al., 1983; Krüger et al., 1985; Gopasyuk, 1985; Stenflo et al., 1987b). Furthermore, quantitative values of the vertical gradient have mainly been restricted to sunspots or their immediate surroundings.

Our diagnostic is built up around the Fe I $\lambda$ 15648.54 Å line ($g = 3$), the centre to limb variation of which has been described by Stenflo et al. (1987b). They discovered the curious fact, that each $\sigma$-component of its Stokes $V$ (which is formed exclusively inside magnetic features to first order) is considerably broader than the complete Stokes I profile, which arises mainly in the non-magnetic atmosphere. The natural explanation is that the $\sigma$-components are significantly broadened by a horizontal or vertical variation of either velocity or magnetic field strength in the magnetic elements (or both). The great sensitivity of the Fe I $\lambda$ 15648.54 Å line to magnetic field gradients is a direct consequence of the large Zeeman splitting of this line. A similar behaviour has been found by Deming et al. (1988) in the case of the Mg I $\lambda$ 12.32 $\mu$m emission line which exhibits broadened $\sigma$-components in sunspot penumbrae. We can understand this broadening of the $\sigma$-components with the help of a very simple model. Consider a vertically constant magnetic field at disk centre whose strength varies horizontally in some prescribed manner. Now consider a line for which the Zeeman splitting $\Delta\lambda_H$ is small compared to its Doppler width, $\Delta\lambda_D$, for all the considered field strengths. The wavelength positions of the $\sigma$-components of this line will be determined only by the non-magnetic width of the line, i.e. no effect of the magnetic field distribution will be visible (as long as the field strength is not correlated to the thermodynamic structure of the atmosphere). This is basically the situation for the lines in the visible spectral range, as far as solar magnetic elements are concerned. When, on the other hand, the Zeeman splitting of the line is larger than its Doppler width, the wavelength positions of its $\sigma$-components will depend on the field strength. If we add the profiles coming from the various field strength regions, the resulting profile will have considerably broader $\sigma$-components. We can also picture the influence of a horizontal distribution of field strengths on a Stokes $V$ profile as the convolution of the $V$ profile formed in a single valued field corresponding to the flux weighted average field strength with a distribution function. The shape of the distribution function is given by the relative amounts of flux at the different field strengths, while its width, for not too strong lines, scales with $\Delta\lambda_H/\Delta\lambda_D$. For vertical variations of the magnetic field strength the situation is more involved, but, for sufficiently weak lines (negligible saturation), it can be described similarly if we require that the magnetic field distribution function is additionally weighted by the contribution function of the line in question.

However, it should be noted that the study of one line alone does not allow us to disentangle the influences of velocity and horizontal and vertical magnetic field variations. Through the intercomparison of four carefully selected lines, two in the visible (formed higher in the atmosphere) and two in the infrared (formed deeper in the atmosphere), the various influences can be separated and constraints can be set on the vertical and horizontal field strength variations, as well as on the line broadening velocity amplitude inside solar magnetic fluxtubes.

## 2. Selected lines and analysis procedure

The analysis procedure is based on four lines. In the visible we make use of the well known line pair Fe I $\lambda$ 5247.06 Å ($g_{\rm eff} = 2$, $\chi_e = 0.09$ eV, $\log g^*f = -4.946$, Blackwell et al., 1979) and $\lambda$ 5250.22 Å ($g = 3$, $\chi_e = 0.12$ eV, $\log g^*f = -4.938$, Blackwell et al., 1979), first introduced for magnetic field strength measurements by Stenflo (1973). $g$ is the Landé factor of a line with a simple Zeeman triplet splitting pattern, $g_{\rm eff}$ the effective Landé factor of an anomalously split line. $\chi_e$ is the excitation potential of the lower level of the transition and $g^*f$ is the statistically weighted oscillator strength. In the infrared we use the Fe I line pair $\lambda$ 15648.54 Å ($g = 3$, $\chi_e = 5.43$ eV, $\log g^*f = -0.54$), and $\lambda$ 15822.81 Å ($g_{\rm eff} = 0.75$, $\chi_e = 5.64$ eV, $\log g^*f = 0.025$). The Fe I line at $\lambda$ 15822.81 Å is chosen because of its much smaller Landé factor ($g = 0.75$), and due to the fact that its excitation potential, wavelength and line strength are sufficiently similar to those of $\lambda$ 15648.54 Å for it to be formed at nearly the same height.

Also, both lines are ideal in the respect that although they are strong enough to give a reasonable signal to noise ratio in Stokes $V$, yet they are sufficiently weak for their line widths to be little affected by saturation and, therefore, the thermal properties of magnetic elements. The temperature dependence of the analysis is reduced even further by the similar parameters ($\chi_e$, line strength) of both lines, which means that they react similarly to changes in temperature. Another important point is that the

$\lambda$ 15648.54 Å line is a very pure Zeeman triplet, with empirical values of $g_l = 3.002$ and $g_u = 2.97$ according to Litzén (1976). $g_l$ and $g_u$ are the Landé factors of the lower and upper levels of the transition, respectively. Therefore, the large widths of its $\sigma$-components cannot be due to anomalous Zeeman splitting. In the following we shall often refer to the strongly split $\lambda$ 15648.54 Å line as the "magnetic" line and to the relatively Zeeman insensitive $\lambda$ 15822.81 Å line as the "Doppler" line.

The analysis procedure is divided into two main parts. The first part is based on the fact that the widths of the $\sigma$-components of the "magnetic" line are very sensitive to vertical and horizontal field strength variations as well as to velocity broadening, while the widths of the $\sigma$-components of the "Doppler" line are only slightly affected by magnetic field variations, but are susceptible to velocity broadening. The use of both lines in an iterative procedure allows the influence of magnetic field and velocity variations to be separated. However, these two lines alone cannot distinguish between a vertical and a horizontal magnetic field gradient. The detailed procedure employed in the first part of the analysis is the following:

(i) A synthetic calculated profile assuming an initial (horizontal, or vertical, or both) magnetic field distribution is fitted to the observed "magnetic" line.

(ii) Next, using this magnetic field distribution the synthetic profile of the "Doppler" line is calculated and Doppler broadened to fit the observed data. The velocity broadening can be determined very accurately at this stage, as the width of this line proves to be largely independent of the used magnetic field distribution. Of course, the Doppler velocity so derived is somewhat model dependent. We follow the concept off micro- and macroturbulence as a description of the velocity broadening in the quiet photosphere (e.g. Evans et al., 1975; Smith et al., 1976; Holweger et al., 1978; Nordlund, 1978), and in fluxtubes (Solanki, 1986).

(iii) The synthetic profile of the "magnetic" line is broadened with the obtained velocity and a new magnetic field distribution is found. Due to the similarity of the two lines it is legitimate to assume that they are broadened by the same velocity.

If necessary, steps (ii) and (iii) can be repeated iteratively, until both observed profiles are reproduced simultaneously. However, this has proved to be unnecessary thanks to the adequate decoupling of the width of the "Doppler" line $\sigma$-components from the Zeeman broadening.

In the second part of the analysis procedure we make use of the fact that Fe I $\lambda$ 5247.1 Å and $\lambda$ 5250.2 Å are formed higher in the atmosphere than the infrared line pair. For the peak of the Stokes $V$ profile of $\lambda$ 5250.2 Å in a 1200 G field and a quiet sun atmosphere Grossmann-Doerth et al. (1988b) find the maximum of the "line depression" contribution function to lie at $\log \tau_{5000} \approx -2.5$. On the other hand, the contribution function of $V$ peak of $\lambda$ 15648.54 Å has its maximum near $\log \tau_{5000} = -1$ (Grossmann-Doerth et al., 1988a). Thus the difference between the field strength derived from the infrared lines and that derived from the visible lines is a measure of the vertical gradient of the field and imposes additional constraints on the magnetic field variation.

We have applied this procedure to two families of fluxtube models. The first family assumes a vertically constant magnetic field in the fluxtube, so that only a radial variation of the field strength may be present. In the other family of models no radial variation is allowed within the fluxtube and the magnetic field is calculated via the thin tube approximation, so that except at the boundary of the tube only a vertical gradient of the magnetic field is present. To account for flux conservation, the fluxtube is allowed to expand with height in this case (the cross-section scaling as $1/B$).

Line profiles are calculated along a set of equidistant, parallel rays piercing the model fluxtube at various positions. If required the rays are weighted according to the area on the solar disk which they represent. The line profiles from all rays are added to give a resultant profile which is compared to the observations. This procedure is often termed 1.5-D radiative transfer.

We carry out this analysis first for the centre of the solar disk (Sect. 4). An approximation we can make within the "thin tube" model family is to consider the contribution of the central ray only (which, in our vertical fluxtube model, corresponds to the fluxtube axis). A comparison between the results of this single ray (1-D) and multiple ray (1.5-D) transfer calculations provides information on the validity of the 1-D approximation for strongly split lines in fluxtubes.

Later we use the models that give us the best fit to the data at disk centre to calculate the line profiles closer to the limb (Sect. 5). It turns out that away from disk centre the Stokes $V$ profile shape of the "magnetic" line is quite sensitive to the assumed fluxtube diameter. If we assume that the fluxtubes have a certain geometry (e.g. slab) and that the magnetic field structure of the fluxtubes is the same in the different regions, then we can set some constraints on the average fluxtube diameters.

## 3. Observational data and model atmospheres

The data used in the present paper were acquired with the McMath telescope and the Fourier transform spectrometer (FTS) polarimeter of the National Solar Observatory at Kitt Peak. Below we briefly summarize some of the main features of the observational data. A detailed description of the data acquisition and reduction has been given by Stenflo et al. (1984, 1987a,b).

We use two spectra each in the visible and in the infrared. The infrared spectra were obtained in a network region at $\mu = 0.99$ and in an active region plage at $\mu = 0.61$. Both spectra have a spatial resolution of 5 arcsec, and a spectral resolving power of approximately 360'000. Their integration times are 53 min and 48 min respectively. The visible spectra are from an enhanced network region at $\mu = 0.98$ (spatial resolution = 10 arcsec, spectral resolving power = 420'000, integration time = 52 min) and an active region plage at $\mu = 0.67$ (spatial resolution = 5 arcsec, spectral resolving power = 523'000, integration time = 43 min).

We are well aware of the problems and pitfalls associated with comparing lines formed in the visible with those formed in the infrared, particularly when the spectra do not refer to the same region, as is the case with our data. However, it is not straightforward to obtain near simultaneous spectra in the visible and the infrared of exactly the same region with the FTS. For example, the difference in refractive index of air between the visible and the infrared means that the position of the spectrograph entrance aperture on the infrared solar image does not correspond to its position on the image seen in the visible. Also, the $\lambda$ 5250/$\lambda$ 5247 line ratio is almost independent of the region observed (Stenflo and Harvey, 1985).

Figure 1 shows the Stokes $I$ and $V$ profiles of the two infrared lines at $\mu = 1.0$ (disk centre) and at $\mu = 0.61$. Both lines

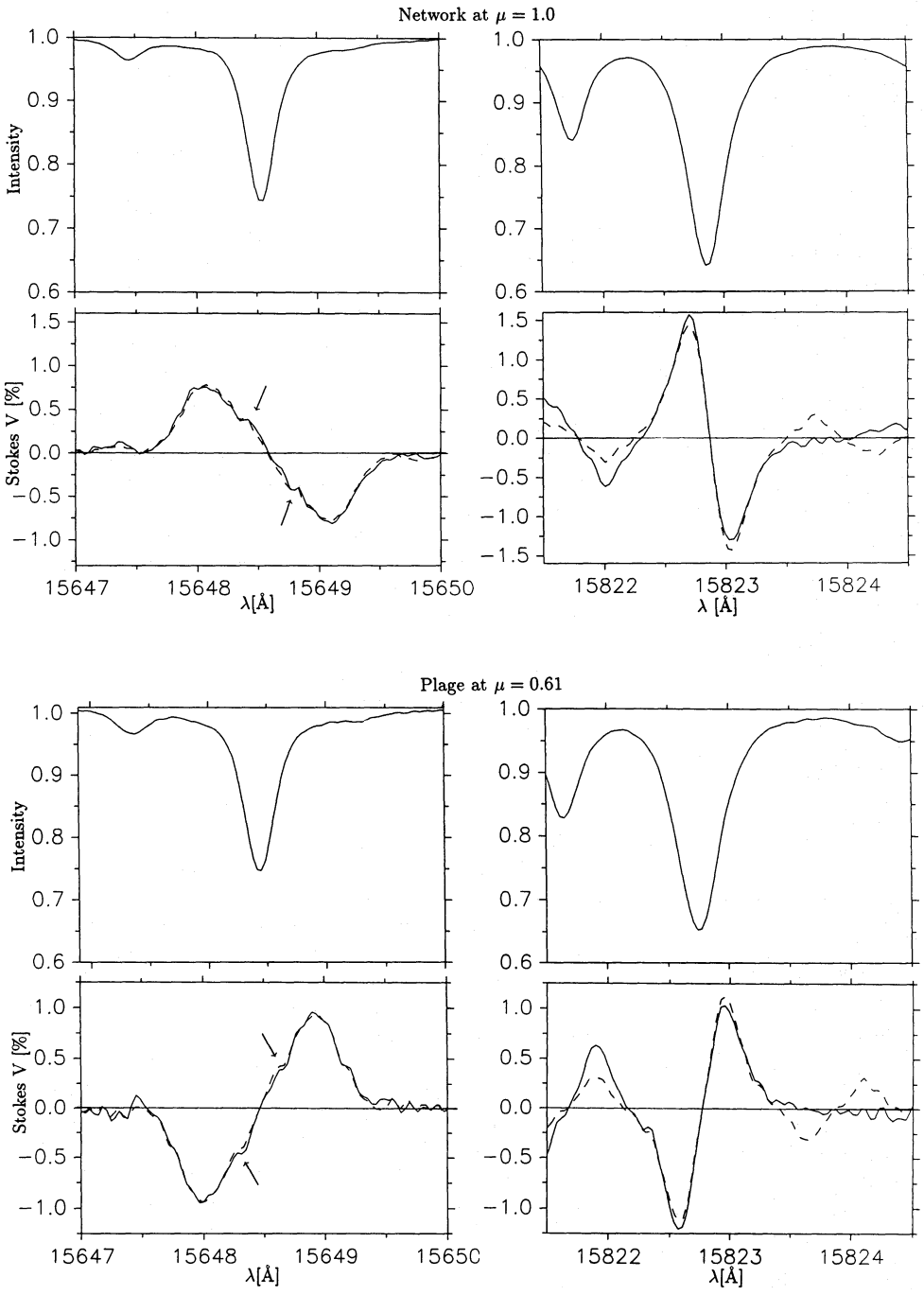


**Fig. 1.** Stokes $I$ and $V$ profiles of the infrared lines $\lambda$ 15648.54 Å ($g = 3$) and $\lambda$ 15822.81 Å ($g_{\text{eff}} = 0.75$) in a network at $\mu = 1$ (upper panels), and a plage at $\mu = 0.61$ (lower panels). Dashed lines are symmetrized Stokes $V$ profiles. The arrows depict the weak field notches

are slightly blended towards shorter wavelengths. The Stokes $V$ profiles have been symmetrized by adding their red and blue wings together (dashed line). The difference between the symmetrized and the observed profiles (solid line) is agreeably small for the "magnetic" line, while for the "Doppler" line the extreme wings of Stokes $V$ appear to be somewhat affected by the blend. Note the large difference between the blue-red asymmetry of the $V$ profiles of the two lines. Such an asymmetry has previously been observed for numerous lines in the visible (e.g. Stenflo et al., 1984; Solanki and Stenflo, 1984, 1985), including Fe I $\lambda$ 5247.1 Å and $\lambda$ 5250.2 Å. Its cause is, so far, not well understood. In view of this we generally fit the symmetrized profiles of the observed lines, except for $\lambda$ 15822.8 Å where, due to the blending of its blue wing, we have preferred to fit only the red wing. However, extensive test fits to the red wings only of all lines have given results very similar to the fits to the symmetrized profiles.

One point of interest of these observed lines is what we call the "weak field notch," which the Stokes $V$ profile of the "magnetic" line exhibits in both spectra (marked by arrows in Fig. 1), and which distinctly lies above the noise level. The fact that the notch is exactly anti-symmetric with respect to the zero-crossing wavelength (it is just as prominent in the symmetrized profile as in the original data) also speaks for the reality of this feature. This notch looks as if it were a superposed weaker and much

less split Stokes $V$ profile, suggesting the existence of a weak magnetic field. Another possible explanation is the presence of a medium strong magnetic field of opposite polarity, which "eats away" part of a Stokes $V$ profile that envelopes the resulting observed profile. The reason why such a feature has never been observed in spectra obtained in the visible, and for that matter is not seen in the $\lambda$ 15822.81 Å line, is the much smaller Zeeman splitting of these lines. As long as a spectral line is not completely split, atmospheric regions with different field strengths will produce profiles whose $\sigma$-components overlap almost completely.

The standard HSRA atmosphere (Gingerich et al., 1971) modified to comply with LTE (Solanki, 1987b) serves as a model of the quiet sun. At disk centre the fluxtube interior is modelled using the network model of Solanki (1986) modified to incorporate results of continuum contrast measurements in the visible (cf. Solanki and Steenbock, 1988). Test calculations employing Solanki's (1986) plage model and the HSRA, respectively, for the magnetic component produced no significant differences in the results. The plage model is used to represent fluxtubes near $\mu = 0.6$, since the observations near that $\mu$ value stem from an active region plage. The main conclusion to be drawn from the test calculations with different temperature structures is that the proposed technique is practically temperature independent as long as only horizontal variations of the magnetic field are assumed. For a vertical this need no longer be the case.

Since in part of our radiative transfer calculations rays passing through both the fluxtubes as well as their immediate surroundings are present, we must specify the atmosphere in the immediate vicinity of the fluxtubes also. Although there is mounting theoretical and observational evidence that the immediate surroundings of the fluxtubes differ considerably from the quiet sun (Spruit, 1977; Deinzer et al., 1984a,b; Nordlund, 1986; Cavallini et al., 1987; Schüssler and Solanki, 1988), no accurate model for their line forming layers exists. Additionally, our analysis is practically independent of filling factors and temperature structures. In view of this we have assumed the HSRA to represent the close non-magnetic surroundings of the fluxtubes as well.

Both the HSRA and the network models have been extended to deeper layers to give suitable models for calculating the infrared lines, whose height of formation is lower than of lines in the visible. In the case of the HSRA this has been done by smoothly attaching Spruits' model of the solar convection zone (Spruit 1974), which is similar to the procedure employed by Chapman (1979). Like him we name the resulting model atmosphere the HSRASP. Electron pressure and absorption coefficient have been determined using the code of Gustafsson (1973). For the fluxtube, for which no extension to greater depths is readily available, a linear extrapolation of temperature, pressure scale height and magnetic field has been adopted after test calculations have shown little or no influence of several parametrized extrapolation curves. Above $\tau_{15000} \approx 1$ the behaviour of the magnetic field strength is determined by the thin tube approximation, i.e. it satisfies horizontal pressure balance, but neglects the effects of magnetic tension. Its absolute value has been fixed by Solanki et al. (1987) through a comparison of calculated Stokes $V$ profiles (using a 1-D model) with the observed $\lambda$ 5250/$\lambda$ 5247 Stokes $V$ line ratio. The curves of temperature and field strength of the models versus the logarithmic continuum optical depth at $\lambda = 15{,}000$ Å are shown in Fig. 2. A height-independent microturbulence of 0.6 km s$^{-1}$ is adopted for the HSRA (cf. Blackwell and Shallis, 1979) and the fluxtube models.

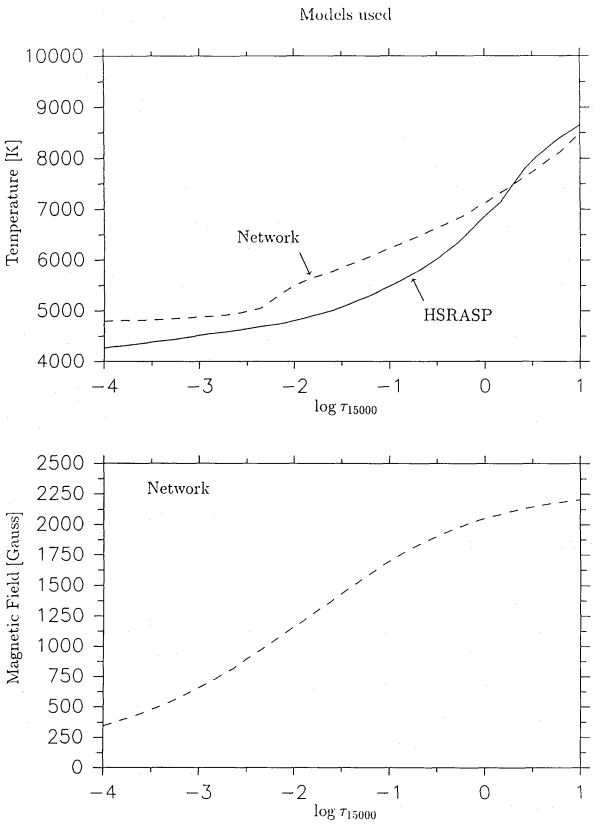


**Fig. 2.** Upper panel: temperature structure of the extended modified HSRASP model (solid curve) and the extrapolated network model of Solanki (dashed curve). Lower panel: vertical magnetic field structure of the network model

We choose −7.5 for the logarithmic abundance of iron and 2.5 for $\delta_\Gamma$ (the empirical correction factor for the Van der Waals damping), as suggested by Holweger (1979).

The line profile calculations are carried out with the modified Stokes radiative transfer code of Beckers (Beckers, 1969a,b; Solanki 1987b). In a first step, the $\log g^*f$ values of both infrared lines, listed in Sect. 2, has to be determined ($g^*f$ being the oscillator strength of the considered transition), as no published values could be found in the literature. Synthetic Stokes $I$ profiles are fitted to the observed $I$ profiles with $\log g^*f$ as a parameter. The HSRASP is used, since the Stokes $I$ profile we observe has its main contribution from the non-magnetic surroundings of the fluxtubes due to the small filling factor in that region (approximately 4%; cf. Sect. 4). Blends must be compensated, if an accuracy of a few percent is to be achieved. Although these $\log g^*f$ values may be slightly too small due to the neglected weakening of the lines in the network, any error should be similar for both lines and should not affect the results.

Using the HSRASP we have also derived the macroturbulence velocity necessary to reproduce the Stokes I line widths. We obtain 2 km s$^{-1}$, so that the total turbulent broadening velocity (root of squared micro- and macroturbulence) seen by these lines is 2.1 km s$^{-1}$.

## 4. Results of the analysis at disk centre ($\mu = 1.0$)

We first attempt to fit the infrared lines with a single component, vertically and horizontally constant, magnetic field of

strength $B_0$ within the fluxtube. For the moment we ignore the weak field notch in the "magnetic" line. Without velocity broadening the calculated Stokes $V$ profiles of both lines are much too narrow, so that some velocity and/or magnetic field broadening must be present. The fit to the "magnetic" line yields $B_0 = 1.5\,\mathrm{kG}$ and $v_{\mathrm{Dop}} = 5\,\mathrm{km\,s^{-1}}$. $v_{\mathrm{Dop}}$ is the Doppler width of the Gaussian macroturbulence profile which must be convoluted to the synthetic line profile to make its $\sigma$-components broad enough to match the observed line profile. However, these parameters give a much too broad Stokes $V$ profile of the "Doppler" line, as is illustrated in the upper panel of Fig. 3. Note that in this and the following figures the calculated Stokes $V$ profiles have been scaled and shifted to improve the match to the data. The "Doppler" line allows a maximum value of $v_{\mathrm{Dop}} = 3.3\,\mathrm{km\,s^{-1}}$, which leads to a much too narrow profile for the "magnetic" line (lower panels of Fig. 3). No $B_0$ and $v_{\mathrm{Dop}}$ pair can be found that simultaneously fits both lines. Since the two infrared lines are not completely identical, the velocities required to reproduce their Stokes $V$ widths may be slightly different, but the lines are too similar for the difference to be almost $2\,\mathrm{km\,s^{-1}}$. Furthermore, the analysis of Stokes $V$ profiles in the visible suggests that weaker lines require smaller broadening velocities (Solanki, 1986), so that one should actually expect the "magnetic" line to be reproducible with a slightly smaller velocity than the "Doppler" line. The simple picture of fluxtubes being "sticks" of vertically and horizontally constant field strength can thus be ruled out; a certain amount of Zeeman broadening is needed to explain the width of the "magnetic" line.

Next, we relax the assumption of a horizontally constant field, i.e. we allow a horizontal variation of field strength. In analogy to the field strength distribution in symmetrical sunspots (e.g. Beckers and Schröter, 1969) Stenflo (1973) suggested a plausible radial magnetic field distribution parametrized by $B_0$, the field strength at the axis of the fluxtube, $r_0$, the radius of the tube, and $\beta$, a measure of the variation of the field strength with distance from the axis:

$$B(r) = B_0(1 - (r/r_0)^2)^{\beta}. \tag{1}$$

For a cylindrical fluxtube Eq. (1) leads to a distribution function $f(B)$ which represents the amount of magnetic flux present in the form of a given field strength, given by:

$$f(B) \sim B^{(1/\beta - 1)}. \tag{2}$$

In addition to this function we made use of a box (i.e. only field strengths within a certain range are present, all of which carry equal amounts of flux) and a Gaussian $f(B)$ distribution function. We find that reproducing the width of the "magnetic" line with only an appropriate field distribution results in a too narrow profile for the "Doppler" line due to its small sensitivity to the magnetic field. Therefore, both Doppler and Zeeman broadening are needed. Such a combined fit to both lines (carried out as described in Sect. 2) yields $v_{\mathrm{Dop}} = 3\,\mathrm{km\,s^{-1}}$. However, as can be seen in Fig. 4, the data do not allow us to distinguish between the various distribution functions. We get $B_0 = 1.9\,\mathrm{kG}$, and $\beta = 0.425$ for the distribution of Eq. (2), $B_0 = 1.5\,\mathrm{kG}$ for the Gaussian with an $e$-folding width of 650 Gauss, whereas the box distribution function spans field strengths from 800 to 2100 Gauss.

Attempts to model the weak field notch are shown in Fig. 5, where the possibilities of it being caused by either a positive (i.e. with the same polarity as the fluxtube field) or a negative background field have been examined. In the first case a field of 400 G carrying 2% of the whole flux is needed, whereas in the second case an inverse field of 800 G with 5% of the flux subtracted from a broader field distribution approximates the observed profile best. The broader enveloping Stokes $V$ profile can be produced by $B_0 = 2.0\,\mathrm{kG}$, and $\beta = 0.675$ using the distribution described by Eq. (2). These numbers are compatible with the results of Howard and Stenflo (1972) and Frazier and Stenflo (1972), who found that over 90% of the net magnetic flux is in strong field form. Of course, a large part of the magnetic field

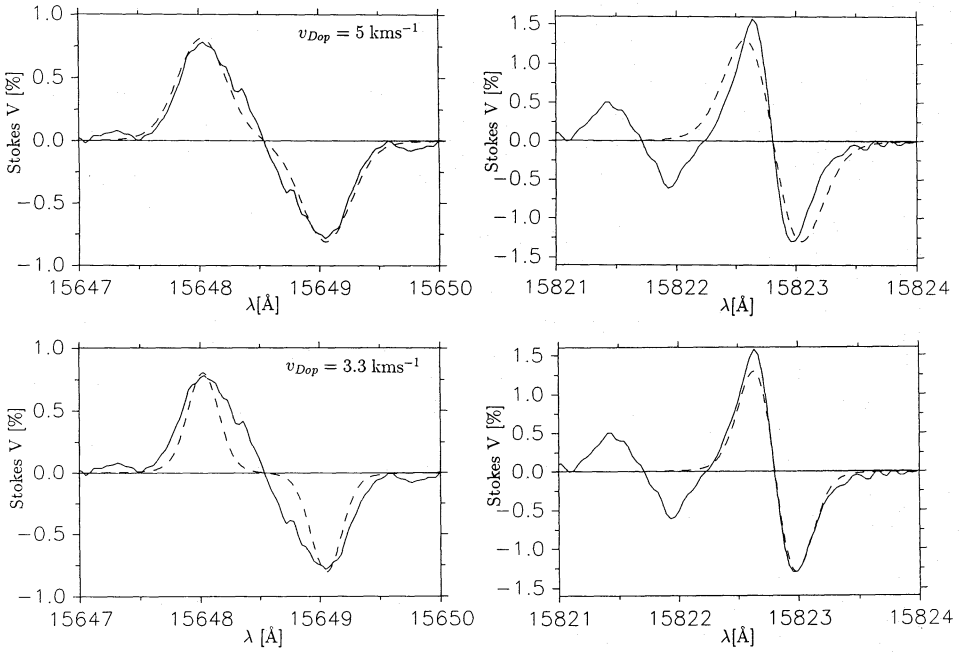


**Fig. 3.** Single component fits to the Fe I $\lambda$ 15648.54 Å ("magnetic") line and the $\lambda$ 15822.81 Å ("Doppler") line with $B = 1.5\,\mathrm{kG}$. A macroturbulence velocity of $v_{\mathrm{Dop}} = 5\,\mathrm{km\,s^{-1}}$ is required by the "magnetic" line (upper panels) whereas the "Doppler" line allows only for a $v_{\mathrm{Dop}} = 3.3\,\mathrm{km\,s^{-1}}$ (lower panels). $\mu = 1$, i.e. disk centre

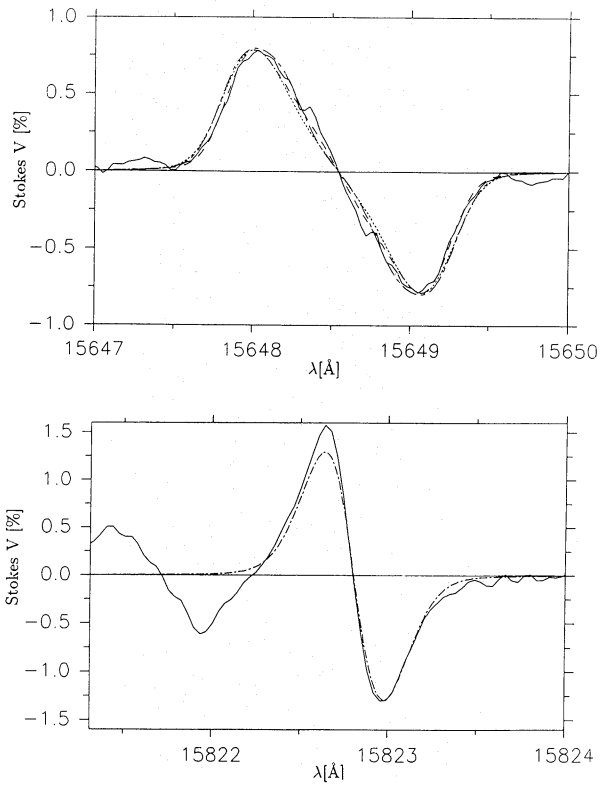


**Fig. 4.** Fits to the "magnetic" line assuming a purely horizontal gradient of the magnetic field, using the distribution function given by Eq. (2) with $B_0 = 1.9\,\mathrm{kG}$, $\beta = 0.425$, and $v_{\mathrm{Dop}} = 3\,\mathrm{km\,s^{-1}}$ (dashed line), a Gaussian with $B_0 = 1.5\,\mathrm{kG}$, $\Delta B_{\mathrm{Dop}} = 0.65\,\mathrm{kG}$ and $v_{\mathrm{Dop}} = 2.8\,\mathrm{km\,s^{-1}}$ (dotted line) and a box distribution function extending from 800 to 2100 G with $v_{\mathrm{Dop}} = 2.75\,\mathrm{km\,s^{-1}}$ (dot-dashed line). For the "Doppler" line all three functions give almost identical profiles; only the line profile resulting from the box distribution has been plotted for reasons of clarity. $\mu = 1$

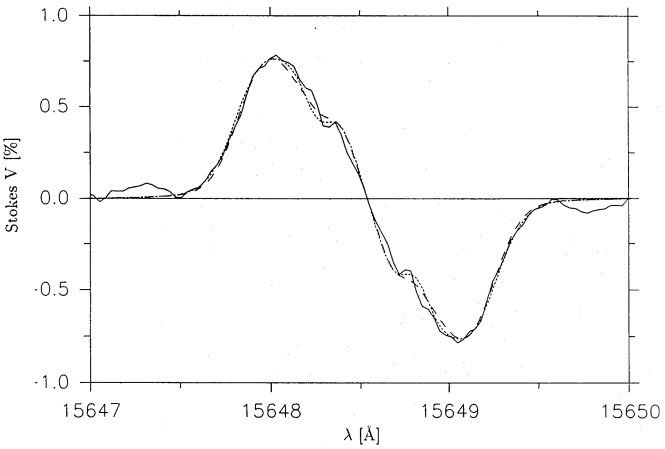


**Fig. 5.** "Additive" and "subtractive" fits to the weak field notch. The distribution function of Eq. (2) is first used to calculate the basic profile. Adding a profile calculated with a constant 400 Gauss field carrying 2% of the flux to the profile of Fig. 4 results in the dashed curve, whereas subtracting a profile calculated with 800 Gauss (carrying 5% of the total flux) from a profile with $B_0 = 2.0\,\mathrm{kG}$ and $\beta = 0.675$ produces the dotted curve. $\mu = 1$

may be in a tangled state on a relatively small scale and, therefore, not readily visible in Stokes $V$ (e.g. Stenflo, 1988). To account for the relative sharpness of the notches, profiles unbroadened by velocities are used for the weak field component. Since we do not have any knowledge of the temperature in this weak field component, we assume it to be equal to that of the fluxtubes and use the network model to calculate the line profiles formed there. The amount of weak field flux derived from the data depends somewhat on this choice. For example, if, instead, we use the HSRASP we obtain 1.4% and 3.3% of the total flux in weak field, respectively medium strong field form.

As pointed out in Sect. 2, the two infrared lines alone are insufficient to distinguish between horizontal and vertical gradients of the magnetic field. As a next step we, therefore, calculate the $\lambda\,5250/\lambda\,5247$ Stokes $V$ line ratio for one of the $f(B)$ distributions which reproduce both infrared lines. We have chosen the distribution given by Eq. (2). The value of 0.75 for the amplitude line ratio found by Stenflo et al. (1987a) cannot be reproduced unless the field strengths of the distribution are reduced by a factor of approximately 0.77. This is a direct indication of a vertical field gradient, as the Stokes $V$ profiles of the $\lambda\,5250.2$ Å and $\lambda\,5247.1$ Å are formed in higher layers of the photosphere. Note that $v_{\mathrm{Dop}}$ has also to be redetermined carefully from the line widths of the $\lambda\,5247/\lambda\,5250$ lines, as it strongly affects the line ratio too (e.g. Solanki et al., 1987). A $v_{\mathrm{Dop}}$ of $2.2\,\mathrm{km\,s^{-1}}$ is needed to fit these lines, a value which is compatible with previous determinations. As the data in the visual do not originate from the same region as those in the infrared, slightly different line ratios may not be surprising, but a 23% discrepancy is significant due to the relatively unique field strength found in solar magnetic fluxtubes with the line ratio technique (cf. Stenflo, 1976; Stenflo and Harvey, 1985).

In order to achieve consistency between the data in the infrared and the visible Solanki's network model is used along with a magnetic field structure calculated under the assumption of a thin fluxtube (cf. Sect. 3 and Fig. 2). A purely one-dimensional calculation is then carried out (no horizontal field distribution, line profiles calculated along a single ray at the fluxtube axis). The result, for $v_{\mathrm{Dop}} = 2.75\,\mathrm{km\,s^{-1}}$, is illustrated in Fig. 6. Clearly, as long as we disregard the weak field notch, the two infrared profiles are equally well reproduced by this vertical magnetic field gradient alone, without further need for broadening by a lateral field variation. It has the additional advantage that it also reproduces the $\lambda\,5250/\lambda\,5247$ line ratio. Of course, a less pronounced field gradient in combination with an appropriate horizontal field strength distribution would also give a satisfactory fit to the infrared data, but we see no need to carry out such calculations, particularly since they would lead to worse fits to the line ratio. The success of the purely one-dimensional (i.e. one line of sight) model is, however, offset by one major disadvantage: it does not conserve flux.

To cope with this violation of physical law in the simplest way, 1.5-D radiative transfer calculations are carried out, i.e. the profiles are calculated along many lines of sight penetrating the fluxtube at different radii and weighted according to their area contribution (cf. Sect. 2). For a fluxtube radius $R_0$ at $\tau_{\mathrm{IR}} = 1$, ($\tau_{\mathrm{IR}}$ is $\tau$ at $\lambda = 1500$ Å in the fluxtube) we have added all contributions out to $3R_0$. This corresponds to a filling factor of 11% if the fluxtubes had adjacent canopies of this size which is a liberal estimate for the filling factor in this region, as can be seen by comparing with the empirically derived value below. Despite the

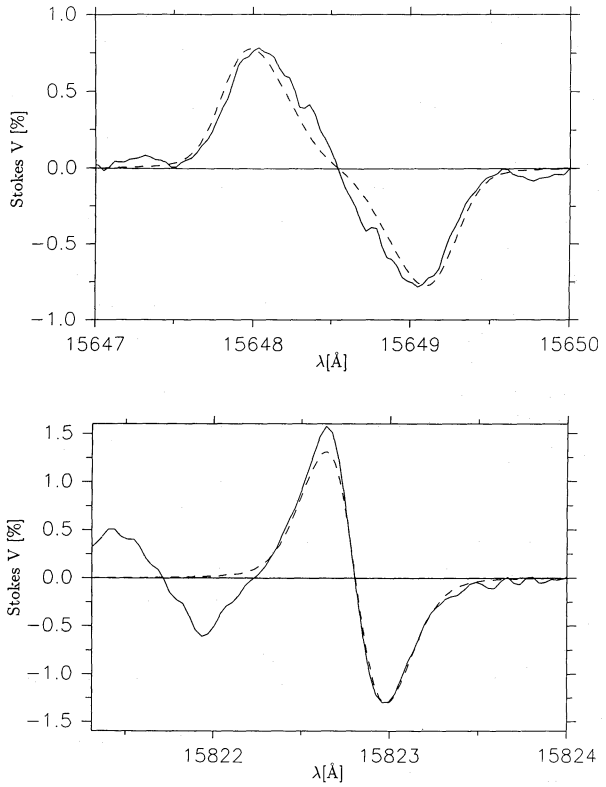


**Fig. 6.** Fit obtained using Solanki's network model with a vertical magnetic field gradient only and a single line of sight along the axis of the fluxtube. $\mu = 1$

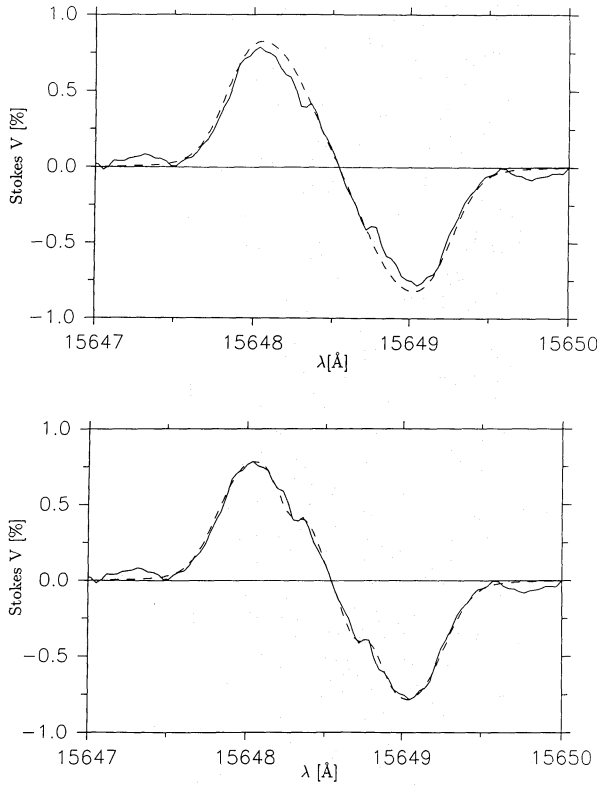


**Fig. 7.** Upper panel: Profile of the "magnetic" line resulting from Solanki's network model in a diverging fluxtube which conserves flux ($B(\tau_{5000} = 1) = 2000$ G and a filling factor of 11% have been assumed). Lower panel: Fit of the weak field notch using two discrete components: an 800 Gauss field of opposite polarity and a 400 Gauss field bearing the same polarity (carrying 5% and 1.5% of the total flux respectively). $\mu = 1$

caution needed when trying to deduce and interpret filling factors (cf. Schüssler and Solanki, 1988), the Stokes $V$ amplitude nevertheless provides an estimate of it, and can be used as a crude check to see whether our assumed value is reasonable. For the infrared data we find approximately 4% which corresponds to a fluxtube canopy extending out to $5R_0$. The contribution of the rays penetrating the fluxtube at this distance from the axis is completely negligible, as is already the case for those around $3R_0$.

The inclusion of flux conservation in the model calculations changes matters considerably: the "magnetic" line grows broader in such a way that the data can only be reproduced in terms of an "outer" fit to the observed line (see Fig. 7). If we are to accept the above model as a description of reality, then we are left with the conclusion that the weak field component has the opposite polarity to the strong field component. A simple way of imagining this is that a certain number of field lines turn back relatively close to the fluxtube much like the branches of a weeping willow (limited return flux). No explicit return flux models for small fluxtubes are known to us, although some sunspot models incorporate this feature (e.g. Flå et al., 1982). This picture does not change significantly even when assuming only a $2R_0$ canopy, corresponding to a filling factor of 20%. We must however bear in mind the fact that a somewhat smaller vertical field gradiet cannot be ruled out, which also results in a smaller fluxtube divergence in our picture, leading to a narrower line profile and thus to an "inner" fit again, i.e. a fit passing to the inside of the weak field notch of the "magnetic" line. A full investigation of this case is outside the scope of the present paper, particularly since we have no a priori reason to prefer either polarity for the weak field component. The best fit to the "magnetic" line, including the weak field notch, is obtained with 5% of the flux having opposite polarity and a field strength of 800 G, and additionally 1.5% of the flux having the same polarity as the fluxtube field and a field strength of 400 G. The fact that we have to use two different magnetic field components to reproduce the observations may be an artifact produced by assuming the background field to be constant, when in reality it may vary with height.

The $\lambda 5250/\lambda 5247$ line ratio calculated with the multi-ray model increases very slightly to 0.77 as compared to 0.75 for the one-dimensional calculations but still remains within the error bars of the observations. The reason for the increase is the greater weight of the weaker fields due to flux conservation. $v_{\mathrm{Dop}}$ decreases somewhat to $1.9\,\mathrm{km\,s^{-1}}$ for the lines in the visible. The inclusion of the weak field has a barely noticeable influence on the $\lambda 5250/\lambda 5247$ line ratio. Thus any field of opposite polarity giving rise to the weak field notch does not have sufficient flux to falsify the conclusions from the $\lambda 5250/\lambda 5247$ line ratio. This contradicts Semel's (1986) suggestion, that relatively weak mixed polarity fields produce the observed line ratio. A smaller vertical magnetic field gradient, as prooposed above to obtain a weak

field of the same polarity as the fluxtubes, may no longer be consistent with the measured line ratio. However, this does not necessarily rule out such a smaller gradient since a change in the fluxtube temperature structure (in particular the temperature gradient), which increases the difference in the heights of formation of the visible and the infrared lines, will make the model consistent with the data. A change in temperature gradient also affects the width of the Stokes $V$ contribution function (B. Larsson, private communication), and thus influences the sensitivity of the "magnetic" line to vertical field gradients. The influence of the temperature structure on the measured magnetic field strength and gradient has previously been pointed out by Schüssler (1987) and Solanki (1987c). Another way in which the temperature structure may affect the analysis is by a horizontal variation of temperatures within the magnetic element. Such a distribution in temperatures may also give rise to a certain broadening of the "magnetic" line, since at various positions in the fluxtube the line will then be formed at different heights and will, therefore, be affected by different field strengths. Moreover, it cannot be ruled out that the "weak field notch" is due to a combination of temperature and magnetic field strength variation in the fluxtube, e.g. at the boundary layer.

## 5. Results derived from data near $\mu = 0.6$

In this section we consider only the "thin tube" model pierced by multiple rays. To be fully consistent with our cylindrical model at disk centre, we would need a three-dimensional calculation of a grid of rays penetrating the fluxtube at the desired angle prior to calculating line profiles away from disk centre. Previous calculations (De Martino, 1986) have, however, revealed that a simple two-dimensional model (with only the lines of sight lying within a single plane being considered) gives sufficiently accurate synthetic Stokes $V$ profiles for many purposes. Such a model has therefore been used to investigate the infrared FTS data obtained at $\mu = 0.61$. We have assumed two different fluxtube geometries with their appropriate divergences:

1) A proper slab model with $R(z) \propto B(z)^{-1}$, where $R(z)$ is the half-width of the slab at height $z$, the slanted lines of sight cut the slab in a plane perpendicular to the direction of translational symmetry. The resulting profile consists of the sum of the contributions from the individual lines of sight.

(b) A cylindrical model with radius $R(z) \propto B(z)^{-1/2}$. Our calculations represent a cut through the central plane of the fluxtube, which also contains the fluxtube axis. Note that this model does not conserve flux exactly. It is possible to partly offset this by weighting the rays individually.

Unlike the case where the lines of sight are vertical, the calculated average Stokes $V$ depends on $R_0$ at $\tau_{IR} = 1.0$. Varying $R_0$ in both of the above model geometries produces two families of models.

We have calculated grids of models of different sizes belonging to families (a) and (b). Figure 8 shows the profiles of the "magnetic" line resulting from the model with $R_0 = 25$, 30, 35, 50 km for family (a) (upper panel), and $R_0 = 50$, 100, 150, 250 km for family (b) (lower panel), together with the observed profile. The influence of this parameter on the resulting profile can be partly understood if we first consider a narrow slab and "pull" it gradually apart towards large $R_0$'s. Consequently, an increasing number of rays come to lie completely within the fluxtube (which, in the limit of very large $R_0$, corresponds to a one-dimensional model

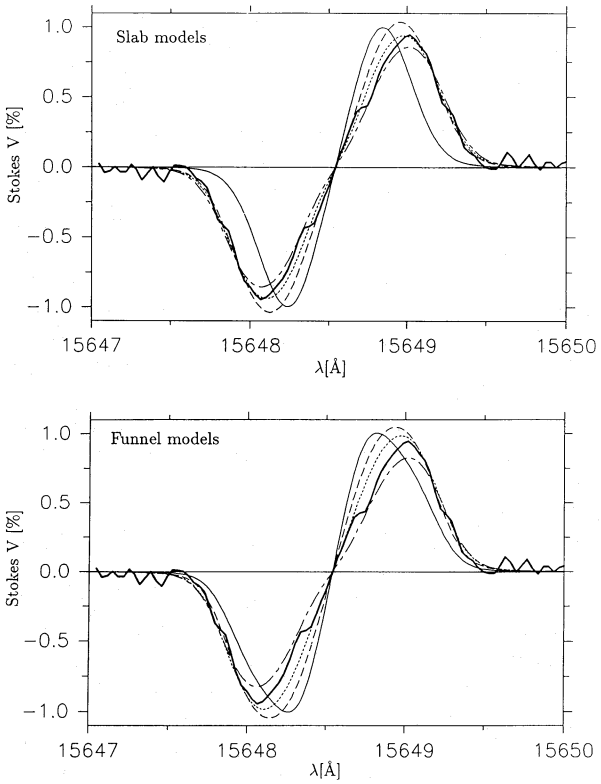


**Fig. 8a and b.** Observations and calculations for $\mu = 0.61$. Observed profile: thick solid line. Upper panel: profiles of the "magnetic" line resulting from model family (a) (slab) with $R_0 = 25$ km (thin solid line), $R_0 = 30$ km (dashed line), 35 km (dotted line), and 50 km (dot-dashed line). Lower panel: profiles from model family (b) (funnel), for $R_0 = 50$ km (thin solid line), 100 km (dashed line), 150 km (dotted line), and 250 km (dot-dashed line)

having a field with a vertical gradient, inclined to the line of sight) thus reducing the relative contribution of the border rays which penetrate only the upper (weaker) fields and then pass into the non-magnetic atmosphere. This should result mainly in a shift of the profile towards larger splitting (i.e. stronger fields).

It follows from Fig. 8 that the models with $R_0 = 30$–$50$ km of family (a) reproduce the line profiles relatively well, as does the model with $R_0 = 150$ km of family (b). Both models also simultaneously reproduce the profile of the $\lambda$ 15822.8 Å line ($v_{Dop} = 3\,km\,s^{-1}$), as well as giving a $\lambda 5250/\lambda 5247$ line ratio of 0.84 ($v_{Dop} = 2\,km\,s^{-1}$), which is in excellent agreement with the observations ($0.83 \pm 0.03$ for $\mu = 0.67$, Stenflo et al., 1987a). Thus a 30 km slab model or a 150 km funnel model fully complies with both data sets. These dimensions are compatible with theoretical results (Schüssler, 1984).

It is disturbing that the difference in geometry should produce such widely different sizes. The most obvious cause for this behaviour is the fact that in the cylindrical case only rays in the central plane are considered. More realistically, rays outside of this plane which see smaller field strengths would also contribute to the average. In an attempt to test whether this is the main cause, the various rays have been weighted individually. However, reasonable amounts of weighting do not affect the derived diameter sufficiently. The only remaining evident source is the difference in fluxtube expansion between the two families of models. Since the slab model expands much more rapidly with

height (in the plane containing the lines of sight), more rays will tend to stay within the fluxtube. Apparently, the proportion of the lines of sight passing into and out of the fluxtube determines the profile of the "magnetic" line. Thee reason for this behaviour is still unclear, but, due to the potential importance of this diagnostic, it will be the subject of future investigations. Another point which suggests that caution is required when interpreting these radii is that the calculations carried out here have assumed a solitary fluxtube, with no neighbours. Although this does not affect the analysis at disk centre, it may play an important role for $\mu \leq 0.67$ ($\theta \geq 54°$). In reality, as we shrink their radii the fluxtubes will, for a fixed filling factor, lie close together so that a single line of sight may pass through more than one fluxtube. This may, to a certain extent, offset the influence of the fluxtube radius on the line profiles. Note that this caveat also applies to the calculations of Van Ballegooijen (1985b) of Stokes $V$ profiles from very thin tubes.

Leaving these problems aside for the moment and considering only one specific geometry it is not a priori to be expected that a single model can fulfill all requirements of both the infrared and the visible data so successfully, at the same time nicely confirming the results of Sect. 4. It forces us to the conclusion that all fluxtubes with the same geometry should have approximately the same dimension. We cannot regard the successful radius within a model family as being a "mean equivalent" radius of a distribution of radii. An attempt to obtain the same profile by adding contributions from different radii leads to a much too broad profile for the "magnetic" line. A chosen geometry thus correlates with an approximate dimension (e.g. half-widths of approximately 30 km for slabs, and a radius of about 150 km for cylindrical fluxtubes). This indicates a possible uniqueness property of fluxtube dimensions. As a consequence, different filling factors would be a result of varying area density of small fluxtubes rather than of their varying horizontal dimension. This result confirms the conclusion of Knölker and Schüssler (1988) that magnetic knots (e.g. Beckers and Schröter, 1968) are not larger fluxtubes with diameters of approximately 1–1.5 arcsec, but, rather, are the observable consequence of the tighter packing of many small fluxtubes. However, a distribution of geometries (or rather expansion rates) with their corresponding dimensions can, of course, not be ruled out. Also, if the field strength in the magnetic elements is correlated to their diameters, such that thinner elements have a larger field strength, then again fluxtubes with a range of fluxtube diameters may be present without broadening the "magnetic" line too strongly. This last point appears unlikely, since for larger structures there is observational evidence for an opposite correlation (sunspots have stronger fields than smaller fluxtubes), which is also in agreement with theoretical arguments. Theoretically, larger fluxtubes are expected to be cooler (less efficent radiative coupling to the surroundings with increasing horizontal optical thickness, cf. Knölker and Schüssler, 1988) with an expanded opacity scale. This allows light from deeper layers in the (larger) fluxtubes, where the field is stronger, to escape.

In view of these uncertainties we prefer to consider the widths of magnetic elements determined here as preliminary.

The "weak field notch" is again best reproduced by an opposite polarity field (return flux picture) with a field strength of 800 Gauss carrying 7% of the total flux irrespective of which family of models, i.e. (a) or (b), is used. The fits are shown in Fig. 9. Note that the fits are far from perfect. However, we are unable to reproduce the line profile any better. This, together with the difficulty in fitting the narrow and sharp weak field notch at $\mu = 1$, may be indicative of shortcomings in the simple weak field interpretation we have proposed. Once more the return flux has only a slight influence on the profiles in the visible. The returning $V$-profiles grow slightly broader, so that $v_{Dop}$ and the line ratio decrease by a negligible amount.

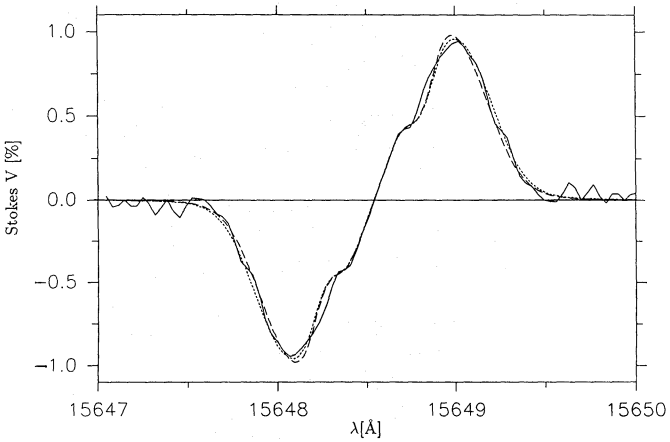


**Fig. 9.** Fit to the weak field notch assuming a 30 km slab model (dashed line) and a 150 km funnel model (dotted line), both with an 800 Gauss field of opposite polarity carrying 7% of the total flux. $\mu = 0.61$

## 6. Conclusions

We have presented a technique for determining magnetic field strength gradients in solar magnetic fluxtubes, which also allows rough limits to be set on fluxtube diameters. It is based on comparing the widths of the individual $\sigma$-components of a strongly Zeeman split line in the infrared with a weakly split, but otherwise similar, line. This allows the broadening due to a possible velocity distribution in solar magnetic fluxtubes to be separated from that caused by a magnetic field variation. By comparing the field strength determined from the infrared lines with that derived from lines in the visible (which are formed higher in the atmosphere), it is also possible to distinguish between vertical and horizontal magnetic field variations. Finally, by carrying out such an analysis at different positions on the solar disk it is also possible to set some preliminary constraints on the dimensions of solar magnetic fluxtubes. In the following we list the main results of the present analysis.

(i) A vertical gradient of the magnetic field strength must be present in solar magnetic fluxtubes. A magnetic field strength decreasing with height in accordance with strict pressure balance (thin tube approximation) reproduces the data relatively well if the field strength at $\tau_{5000} = 1$ is approximately 2000 G, in agreement with the result of Solanki et al. (1987). The $B(\tau)$ curve plotted in Fig. 2 may, therefore, be considered as the best current empirical representation of the behaviour of the magnetic field strength near the center of a magnetic element between $\log \tau = 0$ and $-3$.

(ii) In the lower photosphere the field strength inside the fluxtube must be horizontally nearly constant. This implies that the boundary layer at the edge of the fluxtube cannot be thicker than a relatively small fraction of the fluxtube width, in agreement with the result of Knölker et al. (1988), which they derived from

more indirect arguments. Therefore, current sheet models, such as those of Deinzer et al. (1984a,b) and Steiner et al. (1986) are to be prefered to models having, e.g., a Gaussian horizontal field strength distribution (e.g. Osherovich et al., 1983).

(iii) Most of the fluxtubes in the resolution element must have similar field strengths. This confirms previous results of the line ratio technique by Stenflo and Harvey (1985), who, however, could only show that the variation in *average* fluxtube field strength from one part of the solar surface to another is small.

(iv) At least two distinct components of magnetic flux with different field strengths are present in solar network and active regions. The strong field component corresponds to the traditional fluxtubes with kG fields in the photosphere. The nature of the weaker field component is less certain. If the field strength in fluxtubes does not vary rapidly with height then a magnetic field of the same polarity as the fluxtube field, with a strength of approximately 400 G and containing approximatey 1–2% of the total magnetic flux in the resolution element can explain the observations. However, an opposite polarity field is also possible, and calculations assuming the thin tube approximation to be correct actually suggest that an opposite polarity 700–800 G field with 3–7% of the flux is present. A possible scenario is that a small portion of the field lines of a magnetic fluxtube returns to the solar surface relatively close to the fluxtube (limited return-flux model).

(v) For the studied regions we have, therefore, with the help of our very sensitive technique, confirmed the result of Howard and Stenflo (1972) and Frazier and Stenflo (1972) that over 90% of the *net* magnetic flux outside sunspots is in kilogauss form.

(vi) A sizeable "turbulence" velocity (a combination of micro- and macroturbulence) of 3-3.4 $\mathrm{km\,s^{-1}}$ in magnetic fluxtubes is derived at disk centre from the two infrared lines. This is considerably larger than the "turbulence" velocity in fluxtubes derived from Fe I lines of equal strength in the visible (Solanki, 1986). However, the total "turbulence" velocity in the non-magnetic atmosphere derived from the infrared lines, 2.1 $\mathrm{km\,s^{-1}}$, is also larger than the value derived in the visible from lines of similar strength and excitation potential. This is probably a consequence of seeing deeper into the atmosphere in the infrared.

(vii) The magnetic field strengths and gradients etc. derived at disk centre also satisfy the observations near $\mu = 0.6$, if an appropriate model fluxtube size is chosen.

(viii) If we assume a slab geometry for the fluxtubes (or rather fluxslabs), then the data suggest average fluxtube full widths near the $\tau_{5000} = 1$ level in the fluxtube of between 60–100 km, while for a cylindrical geometry diameters of approximately 300 km result. These values are compatible with the upper limit on the smallest magnetic concentration diameters of 0.3–0.5 arcsec set from direct high resolution observations by Ramsey et al. (1977) and with the limit of 35–105 km derived from the smallest measured magnetic flux by Wang et al. (1985). However, they contradict the lower limit of 390–550 km claimed by Wiehr (1979), also from magnetic flux measurements. We wish to stress that the fluxtube sizes derived here are very preliminary and more work needs to be done to improve the diagnosis of this important fluxtube parameter.

(ix) The small diameters we obtain, even in a relatively strong active region plage, suggest that larger filling factors are often due to the close clumping of many small fluxtubes, rather than to the presence of larger tubes (e.g. Knölker and Schüssler, 1988). This conclusion is reinforced by the fact that once a given geometry for the fluxtubes is assumed (cylindrical or slab) it is found that most fluxtubes in the resolution element must have similar diameters.

(x) The Stokes $V$ profiles of strongly Zeeman split lines calculated using single and multiple lines of sight are quite different. If the resulting profiles are to be compared to spatially averaged observations, then it is important to ensure that the model used conserves magnetic flux with height. For less strongly split lines at disk centre the difference in Stokes $V$ profile *shapes* resulting from radiative transfer calculations along single and multiple lines of sight is considerably smaller. Of course, the Stokes $V$ amplitudes are quite different.

A number of ways of improving, extending and applying the analysis technique developed here come to mind. The most obvious application is to systematically derive field strengths and gradients for a large number of solar regions, to see whether the results of this paper represent the sun as a whole. In particular it would be interesting to apply such an analysis to a young region of emerging flux and observe whether a larger fraction of the flux is present in weak field form. The technique described here can also be applied to high resolution spectra of sunspots, making it possible to map both the horizontal and vertical field distribution simultaneously. Since sunspot fields are stronger, high and low $g$ lines in the visible may partly be used instead of the infrared lines. Such a study should be complementary to the measurements of horizontal field distribution by, e.g., Lites et al. (1988) and Deming et al. (1988).

We wish to stress the importance of using multiple lines having different Zeeman splittings and being formed at different heights, since with a single strongly split line it is not possible to distinguish between various possible broadening mechanisms. A case in point is the observation by Deming et al. (1988) that in sunspot penumbrae the $\sigma$-components of Mg I $\lambda$ 12.32 $\mu$m are broader than its $\pi$-component. They interpret this as a sign of a horizontal distribution of field strengths in the penumbra, after arguing against a vertical magnetic field gradient through a comparison with theoretical models. However, we argue that velocity cannot be ruled out as a cause. If mass motions directed mainly along the field lines are present (as Deming et al. infer from the wavelength shifts of the $\sigma$- and $\pi$-components of the line) and the velocity varies, e.g., along a penumbral fibril or from fibril to fibril, then this would lead to exactly the observed result. When $B$ is nearly parallel to the line of sight the $\sigma$-components are stronger and the velocity is also directed mainly along the line of sight. Therefore, any variation in the velocity will be strongly felt by the line giving rise to broad $\sigma$-components. When the field is almost perpendicular to the line of sight then the $\pi$-component dominates, but since the velocity is now also nearly perpendicular to the line of sight the $\pi$-component will remain relatively narrow.

A future improvement of our analysis must incorporate the Stokes contribution functions of the spectral lines used (Van Ballegooijen, 1985a; Grossmann-Doerth et al., 1988b), since the derived vertical magnetic field gradients depend strongly on the vertical extent of the Stokes $V$ contribution function of the Fe I $\lambda$ 15648.54 Å line as well as on the difference between the heights of formation of the visible and infrared lines, which may be quite temperature dependent.

A straightforward extension of the present analysis would be to consider the line ratio of the complete Fe I $\lambda$ 5247.1 Å and $\lambda$ 5250.2 Å Stokes $V$ profiles. A preliminary analysis, involving only simple Milne-Eddington solutions, by Stenflo (1984) suggests

that useful information on field strength gradients may be derived from an analysis of these lines.

Finally, we would like to repeat the point made by Deming et al. (1988) that observations with a high spectral resolution in the Zeeman regime (i.e. observations of a line with a large Zeeman splitting) can overcome many of the problems posed by the limited spatial resolution of present day observations.

*Acknowledgements.* We are grateful to J.W. Harvey for his assistance in acquiring the FTS data extensively used in this work and to Å. Nordlund for providing the continuum opacity code. The work of one of us (I.Z.) was supported by grants No. 2.666-0.85 and 2.147-0.87 from the Swiss National Science Foundation.

## References

Abdusamatov, H.I.: 1971, *Solar Phys.* **16**, 384
Beckers, J.M.: 1969a, *Solar Phys.* **9**, 372
Beckers, J.M.: 1969b, *Solar Phys.* **10**, 262
Beckers, J.M., Schröter, E.H.: 1968, *Solar Phys.* **4**, 142
Beckers, J.M., Schröter, E.H.: 1969, *Solar Phys.* **10**, 384
Blackwell, D.E., Ibbetson, P.A., Petford, A.D., Shallis, M.J.: 1979, *Monthly Notices Roy. Astron. Soc.* **186**, 633
Blackwell, D.E., Shallis, M.J.: 1979, *Monthly Notices Roy. Astron. Soc.* **186**, 673
Cavallini, F., Ceppatelli, G., Righini, A.: 1987, *Astron. Astrophys.* **173**, 155
Chapman, G.A.: 1979, *Astrophys. J.* **232**, 923
Defouw, R.J.: 1976, *Astrophys. J.* **209**, 266
Deinzer, W., Hensler, G., Schüssler, M., Weisshaar, E.: 1984a, *Astron. Astrophys.* **139**, 426
Deinzer, W., Hensler, G., Schüssler, M., Weisshaar, E.: 1984b, *Astron. Astrophys.* **139**, 435
Deming, D., Boyle, R.J., Jennings, D.E., Wiedemann, G.: 1988, *Astrophys. J.* **333**, 978
De Martino, S.: 1986, *Diplomarbeit*, ETH, Zürich
Evans, J.C., Ramsey, L.W., Testerman, L.: 1975, *Astron. Astrophys.* **42**, 237
Flå, T., Osherovich, V.A., Skumanich, A.: 1982, *Astrophys. J.* **261**, 700
Frazier, E.N., Stenflo, J.O.: 1972, *Solar Phys.* **27**, 330
Frazier, E.N., Stenflo, J.O.: 1978, *Astron. Astrophys.* **70**, 789
Gingerich, O., Noyes, R.W., Kalkofen, W., Cuny, Y.: 1971, *Solar Phys.* **18**, 347
Gopasyuk, S.I.: 1985, *Izv. Krymsk. Astofiz. Obs.* **72**, 159
Grossmann-Doerth, U., Knölker, M., Schüssler, M., Weisshaar, E.: 1988a, in *Solar and Stellar Granulation*, Proc. 3rd International Workshop of the OAC, Capri, June 21–25, 1988 (in press)
Grossmann-Doerth, U., Larsson, B., Solanki, S.K.: 1988b, *Astron. Astrophys.* **204**, 266
Gustafsson, B.: 1973, *Uppsala Astron. Obs. Ann.* **5**, No. 6
Hagyard M.J., Teuber, D., West, E.A., Tandberg-Hanssen, E., Henze, W., Beckers, J.M., Bruner, M., Hyder, C.L., Woodgate, B.E.: 1983, *Solar Phys.* **84**, 13
Harvey, J.W.: 1977, in *Highlights of Astronomy*, ed. E.A. Müller, Vol. 4, Part II, p. 223
Harvey, J.W., Hall, D.: 1975, *Bull. Amer. Astron. Soc.* **7**, 459
Hasan, S.S.: 1985, *Astron. Astrophys.* **143**, 39
Henze, W., Jr., Tandberg-Hanssen, E., Hagyard, M.J., Woodgate, B.E., Shine, R.A., Beckers, J.M., Bruner, M., Gurman, J.B., Hyder, C.L., West, E.A.: 1982, *Solar Phys.* **81**, 231
Holweger, H.: 1979, in *Proc. 22nd Liège International Astrophys. Symp.*, Indst. d'Astrophysique, Liège, p. 117
Holweger, H., Gehlsen, M., Ruland, F.: 1978, *Astron. Astrophys.* **70**, 537
Howard, R.W., Stenflo, J.O.: 1972, *Solar Phys.* **22**, 402
Knölker, M., Schüssler, M.: 1988, *Astron. Astrophys.* **202**, 275
Knölker, M., Schüssler, M., Weisshaar E.: 1988, *Astron. Astrophys.* **194**, 257
Krüger, A., Hildbrandt, J., Fürstenberg, F.: 1985, *Astron. Astrophys.* **143**, 72
Lites, B.W., Skumanich, A., Rees, D.E., Murphy, G.A.: 1988, *Astrophys. J.* **330**, 493
Litzén U.: 1976, *Physica Scripta* **14**, 165
Nordlund, Å.: 1978, in *Astronomical Papers dedicated to Bengt Strömgren*, eds. A. Reiz, T. Andersen, Copenhagen University Obs., p. 95
Nordlund, Å.: 1986, in *Proc. Workshop on Small Magnetic Flux Concentrations in the Solar Photosphere*, eds. W. Deinzer, M. Knölker, H.H. Voigt, Vandenhoeck & Ruprecht, Göttingen, p. 83
Osherovich, V.A., Flå, T., Chapman, G.A.: 1983, *Astrophys. J.* **286**, 412
Pneuman, G.W., Solanki, S.K., Stenflo, J.O.: 1986, *Astron. Astrophys.* **154**, 231
Ramsey, H.E., Schoolman, S.A., Title, A.M: 1977, *Astrophys. J.* **215**, L41
Roberts, B., Webb, A.R.: 1979, *Solar Phys.* **64**, 77
Robinson, R.D., Worden, S.P., Harvey, J.W.: 1980 *Astrophys. J.* **236**, L155
Schüssler, M.: 1984, *Astron. Astrophys.* **140**, 453
Schüssler, M.: 1987, in *Proc. The Role of Fine-Scale Magnetic Fields on the Structure of the Solar Atmosphere*, eds. E.H. Schröter, M. Vázquez, A.A. Wyller, Cambridge University Press, p. 223
Schüssler, M., Solanki, S.K.: 1988, *Astron. Astrophys.* **192**, 338
Semel, M.: 1986, in *Small Scale Magnetic Flux Concentrations in the Solar Photosphere*, eds. W. Deinzer, M. Knölker, H.H. Voigt, Vandenhoeck & Ruprecht, Göttingen, p. 39
Smith, M.A., Testerman, L., Evans, J.C.: 1976, *Astrophys. J.* **207**, 308
Solanki, S.K.: 1986, *Astron. Astrophys.* **168**, 311
Solanki, S.K.: 1987a, in *The Role of Fine-Scale Magnetic Fields on the Structure of the Solar Atmosphere*, eds. E.H. Schröter, M. Vázquez, A.A. Wyller, Cambridge University Press, p. 67
Solanki, S.K.: 1987b, *Ph.D. Thesis*, ETH, Zürich
Solanki, S.K.: 1987c, in *Proc. Tenth European Regional Astronomy Meeting of the IAU*, Vol. 1: *The Sun*, eds. L. Hejna, M. Sobotka, Publ. Astron, Inst. Czechoslovak Acad. Sci., p. 95
Solanki, S.K., Keller, C., Stenflo, J.O.: 1987, *Astron. Astrophys.* **188**, 183
Solanki, S.K., Steenbock, W.: 1988, *Astron. Astrophys.* **189**, 243
Solanki, S.K., Stenflo, J.O.: 1984, *Astron. Astrophys.* **140**, 185
Solanki, S.K., Stenflo, J.O.: 1985, *Astron. Astrophys.* **148**, 123
Spruit, H.C.: 1974, *Solar Phys.* **34**, 277
Spruit, H.C.: 1976, *Solar Phys.* **50**, 269
Spruit, H.C.: 1977, *Solar Phys.* **55**, 3

Spruit, H.C.: 1979, *Solar Phys.* **61**, 363
Steiner, O., Pneuman, G.W., Stenflo, J.O.: 1986, *Astron. Astrophys.* **170**, 126
Stenflo, J.O.: 1973, *Solar Phys.* **32**, 41
Stenflo, J.O.: 1976, in *Basic Mechanisms of Solar Activity*, eds. V. Bumba, J. Kleczek, *IAU Symp.* **71**, 69
Stenflo, J.O.: 1984, *Adv. Space Res.* **4**, 5
Stenflo, J.O.: 1988, *Solar Phys.* **114**, 1
Stenflo, J.O., Harvey, J.W.: 1985, *Solar Phys.* **95**, 99
Stenflo, J.O., Harvey, J.W., Brault, J.W., Solanki, S.K.: 1984, *Astron. Astrophys.* **131**, 333
Stenflo, J.O., Solanki, S.K., Harvey, J.W.: 1987a, *Astron. Astrophys.* **171**, 305
Stenflo, J.O., Solanki, S.K., Harvey, J.W.: 1987b, *Astron. Astrophys.* **173**, 167
Tarbell, T.D., Title, A.M.: 1976, *Solar Phys.* **47**, 563
Tarbell, T.D., Title, A.M.: 1977, *Solar Phys.* **52**, 13
Van Ballegooijen, A.A.: 1985a, in *Measurements of Solar Vector Magnetic Fields*, ed, M.J. Hagyard, NASA Conf. Publ. 2374, p. 322
Van Ballegooijen, A.A.: 1985b, in *Theoretical Problems in High Resolution Solar Physics*, ed. H.U. Schmidt, Max-Planck-Institut für Astrophysik, München, p. 167
Wang, J., Zirin, H., Shi, Z.: 1985, *Solar Phys.* **98**, 241
Wiehr, E.: 1978, *Astron. Astrophys.* **69**, 279
Wiehr, E.: 1979, *Astron. Astrophys.* **73**, L19